The HIV-1 Leader RNA Conformational Switch Regulates RNA Dimerization but Does Not Regulate mRNA Translation†

Truus E. M. Abbink, Marcel Ooms, P. C. Joost Haasnoot, and Ben Berkhout*

Department of Human Retrovirology, Academic Medical Center, University of Amsterdam, Amsterdam, The Netherlands

Received February 11, 2005; Revised Manuscript Received April 19, 2005

ABSTRACT: The untranslated leader RNA is the most conserved part of the human immunodeficiency virus type I (HIV-1) genome. It contains many regulatory motifs that mediate a variety of steps in the viral life cycle. Previous work showed that the full-length leader RNA can adopt two alternative structures: a long distance interaction (LDI) and a branched multiple-hairpin (BMH) structure. The BMH structure exposes the dimer initiation site (DIS) hairpin, whereas this motif is occluded in the LDI structure. Consequently, these structures differ in their capacity to form RNA dimers in vitro. The BMH structure is dimerization-competent, due to DIS hairpin formation, but also presents the splice donor (SD) and RNA packaging (Ψ) hairpins. In the LDI structure, an extended RNA packaging (Ψ^E) hairpin is folded, which includes the splice donor site and *gag* coding sequences. The *gag* initiation codon is engaged in a long distance base pairing interaction with sequences in the upstream U5 region in the BMH structure, thus forming the evolutionarily conserved U5−AUG duplex. Therefore, the LDI−BMH equilibrium may affect not only the process of RNA dimer formation but also translation initiation. In this study, we designed mutations in the 3′-terminal region of the leader RNA that alter the equilibrium of the LDI−BMH structures. The mutant leader RNAs are affected in RNA dimer formation, but not in their translation efficiency. These results indicate that the LDI−BMH status does not regulate HIV-1 RNA translation, despite the differential presentation of the *gag* initiation codon in both leader RNA structures.

The function of noncoding RNAs is often determined by their structure, and some of these RNA molecules make use of conformational changes to regulate their function. An external factor, for instance, a protein or metabolic ligand, is usually required to induce an RNA switch. RNA switches have been implicated in the regulation of various important processes such as alfalfa mosaic virus replication, hepatitis delta virus ribozyme function, and bacterial gene expression (*1*−*4*). The untranslated leader RNA of the human immunodeficiency virus type 1 (HIV-1)[1] can adopt two mutually exclusive structures in vitro (Figure 1) and may therefore function as a molecular switch during the viral life cycle (*5*−*7*). The full-length leader RNA is the most conserved part of the HIV-1 genome and is involved in many steps of virus replication. It contains several sequence and structure motifs (Figure 1) that are involved in early (transcription, splicing, and translation) or late replication steps (RNA dimerization, packaging, and reverse transcription). The proposed RNA switch mechanism may thus allow regulation and appropriate timing of the different leader functions. For instance, the HIV-1 genomic RNA must be translated into the Gag and Gag-Pol proteins prior to RNA packaging into new virions. An RNA switch model was recently also proposed for RNA dimerization of the type C retrovirus Moloney murine leukemia virus (*8*).

The HIV-1 leader RNA consists of an upstream repeat (R) region that recurs at the 3′-terminus of the HIV-1 genome and that comprises the transactivation response (TAR) element and the polyadenylation signal (polyA). The well-characterized TAR hairpin mediates transcription activation by binding of the viral Tat protein and the cellular protein cyclin T (*9*−*17*). The polyA hairpin prevents premature polyadenylation of the nascent RNA by masking of the AAUAAA polyadenylation signal (*18*, *19*). Downstream of R, two important signals for reverse transcription initiation are located: the primer activation signal (PAS) and the primer binding site (PBS) (*20*, *21*). Additional essential motifs are located further downstream in the leader. These include the RNA dimer initiation signal (DIS), the major splice donor site (SD), and the packaging signal (Ψ) that is required for the packaging of the full-length genomic RNA into new virus particles (*22*−*30*).

The energetically favored leader RNA structure is formed by a long distance base pairing interaction between the polyA and DIS motifs and is therefore termed the long distance interaction (LDI) conformation (*7*). The same polyA and DIS motifs fold hairpins in the alternative folding that is termed the branched multiple hairpins (BMH) conformation. The

† RNA studies in the laboratory of B.B. are supported by the NWO-CW (TOP grant) and ZonMw (Vici program).

* To whom correspondence should be addressed: Department of Human Retrovirology, Academic Medical Center, University of Amsterdam, Meibergdreef 15, 1105 AZ Amsterdam, The Netherlands. Telephone: 31 20 566 4822. Fax: 31 20 691 6531. E-mail: b.berkhout@amc.uva.nl.

[1] Abbreviations: HIV-1, human immunodeficiency virus type 1; LDI, long distance interaction; BMH, branched multiple hairpins; DIS, dimer initiation signal; SD, splice donor; R, repeat region; TAR, transactivation response element; polyA, polyadenylation signal; PAS, primer activation signal; PBS, primer binding site; NC, nucleocapsid; KLD, kissing loop dimer; ED, extended dimer(s); Ψ^E, extended Ψ; LTR, long terminal repeat; PCR, polymerase chain reaction; wt, wild-type.

10.1021/bi0502588 CCC: $30.25
Published on Web 06/02/2005

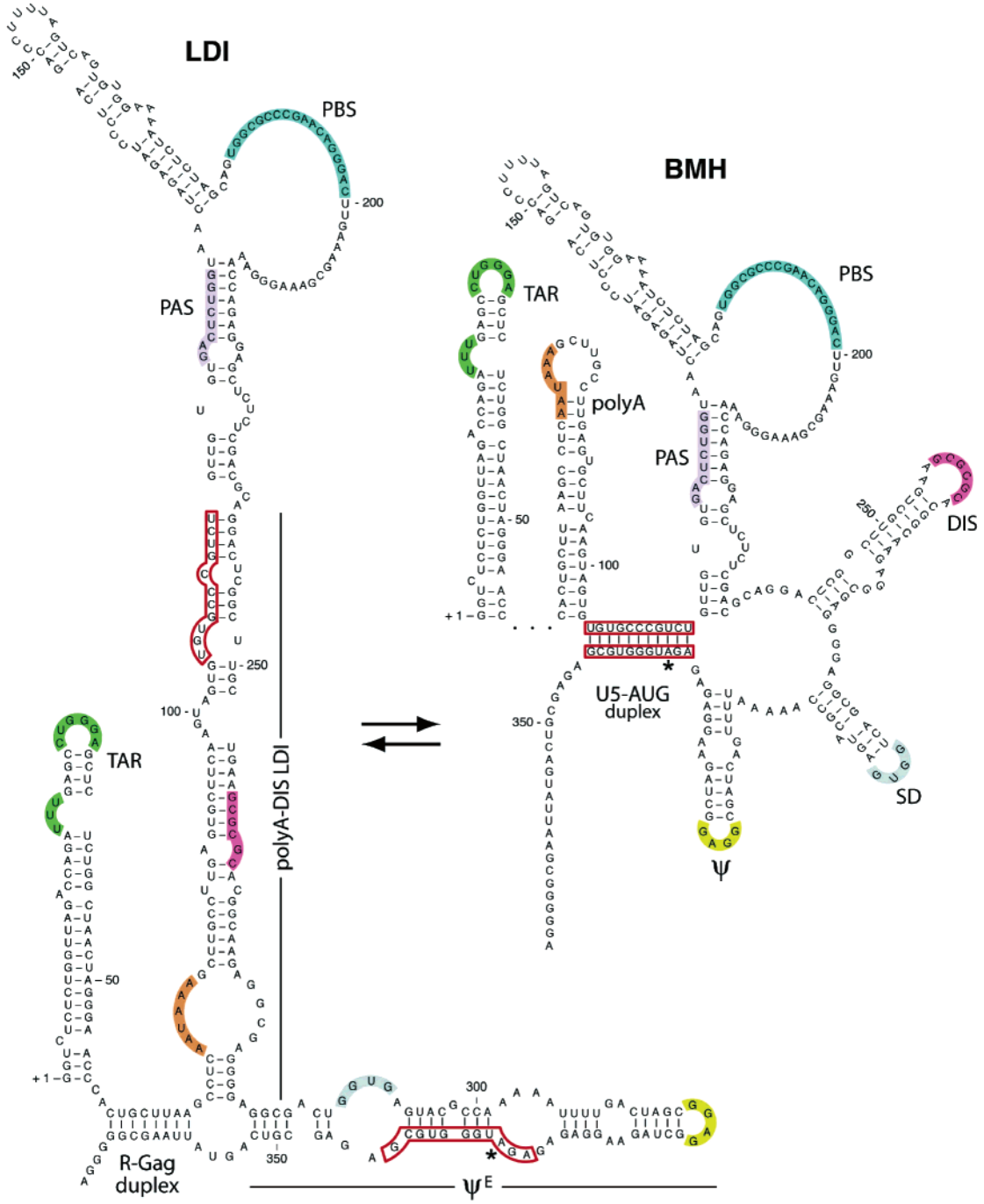

FIGURE 1: Overview of the LDI and BMH structures of HIV-1 leader RNA. The RNA structure models were published previously (*6*). The regulatory motifs are marked in color; see the text for abbreviations.

BMH fold exposes a palindrome sequence in the loop of the DIS hairpin. As a consequence, the BMH can dimerize by formation of an intermolecular kissing loop interaction between the palindromes of two DIS hairpins (*22*, *31*−*36*). This structure is termed the kissing loop dimer (KLD) complex. Subsequently, the two DIS hairpin stems can rearrange such that the intermolecular duplex is extended. This extended dimer (ED) is more thermally stable than the kissing loop dimer (*36*−*38*). Heat treatment or incubation with the viral nucleocapsid protein (NC) triggers ED formation in vitro (*22*, *31*, *34*, *36*, *38*). The LDI structure cannot form RNA dimers because it does not present the DIS hairpin (*7*). Interestingly, NC also induces the conformational shift from LDI to BMH (*7*). These observations strongly suggest that the LDI−BMH switch may provide the virus with a means of regulating RNA dimerization.

More recently, the RNA packaging signal Ψ was also shown to be differently folded in the BMH and LDI folds (*6*). Base pairing occurs between the SD region and 5′ Gag coding sequences in the LDI structure, which leads to extension of the well-known Ψ hairpin (Ψ^E). In contrast, this RNA sequence folds the two discrete SD and Ψ hairpins in the BMH structure. A recent study evaluated more than 30 HIV-1 leader mutants and described a correlation between the status of the LDI−BMH equilibrium and RNA packaging (*5*, *39*−*41*). Possibly, the LDI−BMH switch coordinates the processes of RNA dimer formation and RNA packaging (*5*). Additionally, the LDI−BMH switch could influence the

Table 1: PCR Primers Used in This Study

primer[a]	primer sequence (5′ → 3′)[b]
T7-2	CTAATACGACTCAGTATAGGGTCTCTCTGGTTAGACCAG
TA010	GGGAACAAAAGCTGGG
TA014	TCTTCCATGGTATCTTTATCATCATCATCTTTATAATCTC-CCCCTGGCCTTAACCG
J1 r	CAAAATTTTTGG▲GT***G***C***G***CACCAGTCGCCTCCCC
J1 f	GGTG***C***G***C***AC▲CCAAAAATTTTGACTAGCGGAGGCT
J2 r	AGTCAAAA***AGGA***TGGCGTACTCACCAGTCGCC
J2 f	GAGTACGCCA***TCCT***TTTTGACTAGCGGAGGCTAGAAGG
J3 r	AGTCAAAA***CCCC***TGGCGTACTCACCAGTCGCC
J3 f	ACGCCA***GGGG***TTTTGACTAGCGGAGGCTAGAAGG
J4 r	AGCCTCCGCTAG***AA***AAAATTTTTGGCGTACTCACC
J4 f	TTT***TT***CTAGCGGAGGCTAGAAGGAG
J5 r	AGCCTCCGCTAG***CT***AAAATTTTTGGCGTACTCACC
J5 f	TTT***AG***CTAGCGGAGGCTAGAAGGAG
J6 r	TTTTTGGCGTACTCACCAG▲CG***T***C***A***CCCCTCGCCTCTTG
J6 f	GACGCTGGTGAGTACGCCAAAAATTTTG
J7 r	CAAAATTTT***A***GGCG▲ACTCACCAGTCGCC
J7 f	GAGT▲CGCC***T***AAAATTTTGACTAGCGGAGGCTAG
J8 r	CAGCAAGCCGAG***GGG***TGCGTCGAGAGAGCTCCTC
J8 f	CGACGCA***CCC***CTCGGCTTGCTGAAGCGCGC
J9 r	ACTCACCAGTCGCCT***GGA***CTCGCCTCTTGCCGTG
J9 f	***CC***AGGCGACTGGTGAGTACGCC

[a] f denotes the forward primer; r denotes the reverse primer. [b] Nucleotide changes are indicated in bold italic type; nucleotide deletions are denoted with filled triangles.

process of translation initiation. The *gag* initiation codon is differently folded in the LDI and BMH structure (*6*). It is involved in an evolutionarily conserved long distance base pairing interaction with U5 sequences (U5−AUG duplex) in BMH folding, whereas it is part of an internal loop in the LDI structure (Figure 1). The LDI−BMH equilibrium was therefore suggested to regulate translation initiation (*6*). To test this hypothesis, we constructed a set of 10 leader mutants (J1−J10) that alter the LDI−BMH equilibrium, and thus the structural presentation of the DIS palindrome and the *gag* initiation codon. We determined the effect of these mutations on RNA dimer formation and mRNA translation efficiency.

MATERIALS AND METHODS

Constructs. The plasmid Blue-5′LTR was used for mutation of the HIV-1 leader RNA (*42*). This pBluescript-derived construct contains the *Xba*I−*Cla*I fragment of the infectious pLAI clone, including the 5′ long terminal repeat (LTR) promoter sequence, the full-length leader sequence, and part of the Gag open reading frame (−454/+376, relative to the transcriptional start site at position +1). Mutations were created by a polymerase chain reaction (PCR) method. For construction of the J1−J9 mutations, we used oligonucleotide primers that are listed in Table 1. The J10 mutant was made by combination of the J8 and J9 mutations. Forward primers were used in combination with TA010 and reverse primers with T7-2. PCR products from these reactions were isolated from the agarose gel and used as overlapping templates in a PCR with primers T7-2 and TA010. The resulting PCR products were digested with *Hin*dIII and *Cla*I and cloned into the Blue-5′LTR vector. Introduction of the mutation into the cloned fragments was confirmed by sequencing. The *Xba*I−*Cla*I fragments were subsequently cloned into pLAI-R37, a derivative of the full-length infectious clone pLAI (*43*). The mutant proviral constructs were designated pLAI-J1−pLAI-J10.

The wild-type and mutant pLAI constructs were used as templates in a standard PCR with primers T7-2 and TA014. The PCR products were digested with *Nco*I and *Hin*dIII and inserted into the pBlue-3′LTR−luciferase reporter construct (*44*). The resulting constructs (pLTR-gag-flag-luc-J1−pLTR-gag-flag-luc-J10) contain the HIV-1 5′ LTR promoter region, the complete RNA leader, nucleotides 1−75 of the Gag coding sequence, an in-frame FLAG coding sequence, and the firefly luciferase open reading frame. The protein that is expressed from this luciferase reporter plasmid is a fusion product of the 25 N-terminal Gag amino acids followed by the Flag peptide (amino acids DYKDDDDKD) and the firefly luciferase protein.

The pRL-CMV plasmid contains the *Renilla* luciferase reporter gene under control of the CMV promoter (Promega). pcDNA3-Tat (*45*) expresses the HIV-1 LAI tat gene under control of the CMV promoter and is a derivative of the pcDNA3 vector (Invitrogen). The pSYNGP vector expresses the Gag and Gag-Pol polyproteins and was a kind gift of S. Kingsman (*46*).

RNA Secondary Structure Prediction. Computer-assisted RNA secondary structure predictions were performed using the Mfold version 3.0 algorithm (*47*, *48*) offered by the MBCMR Mfold server (mfold.burnet.edu.au/). Standard settings were used for all folding jobs (37 °C and 1.0 M NaCl). Folding was performed with sequences comprising nucleotides 1−368 of the genomic RNA sequence of the wild-type and mutant HIV-1 leader RNA.

In Vitro Transcription and RNA Dimerization. The pLAI-based set of plasmids were used as templates in a PCR with primers T7-2 and R:A368-A347 (complementary to residues 368−347 of the HIV-1 genome). The PCR products were precipitated with ethanol and used for in vitro transcription with the megashortscript T7 transcription kit (Ambion) in the presence of 1 μL of [α-^{32}P]UTP (0.33 MBq/μL, Amersham Biosciences) according to the manufacturer's instructions. Transcription reaction mixtures were incubated for 3 h at 37 °C and reactions stopped by DNase treatment. Subsequently, formamide-containing loading buffer was added. The RNA was purified on a 4% denaturing polyacrylamide gel. Bands were visualized by autoradiography and excised from the gel. The RNA was eluted overnight in water at room temperature, precipitated with ethanol, and dissolved in water. RNA was quantified by scintillation counting, and the samples were stored at −20 °C. Dimerization was performed with 20 ng of ^{32}P-labeled RNA in 24 μL of dimerization buffer [83 mM Tris-HCl (pH 7.5), 125 mM KCl, and 5 mM $MgCl_2$]. The mixture was heated for 2 min at 85 °C, incubated for 10 min at 65 °C, and slowly cooled to room temperature for renaturing and dimerization. Samples were analyzed on 4% nondenaturing polyacrylamide gels in 0.25× TBE (22.5 mM Tris, 22.5 mM boric acid, and 0.5 mM EDTA) or 0.25× TBM (22.5 mM Tris, 22.5 mM boric acid, and 0.1 mM $MgCl_2$), with a nondenaturing loading buffer (30% glycerol with bromophenol blue). Electrophoresis was performed at room temperature (150 V). Furthermore, 20 ng of ^{32}P-labeled RNA was incubated for 5 min at 85 °C in formamide-containing loading buffer (Ambion) and analyzed on a 6% denaturing polyacrylamide gel. All gels were dried and subjected to autoradiography. Quantification of the percentage dimerization was performed on a PhosphorImager (Molecular Dynamics). The dimerization yield was determined by dividing the amount of dimer by the total amount of RNA (dimer and monomer).

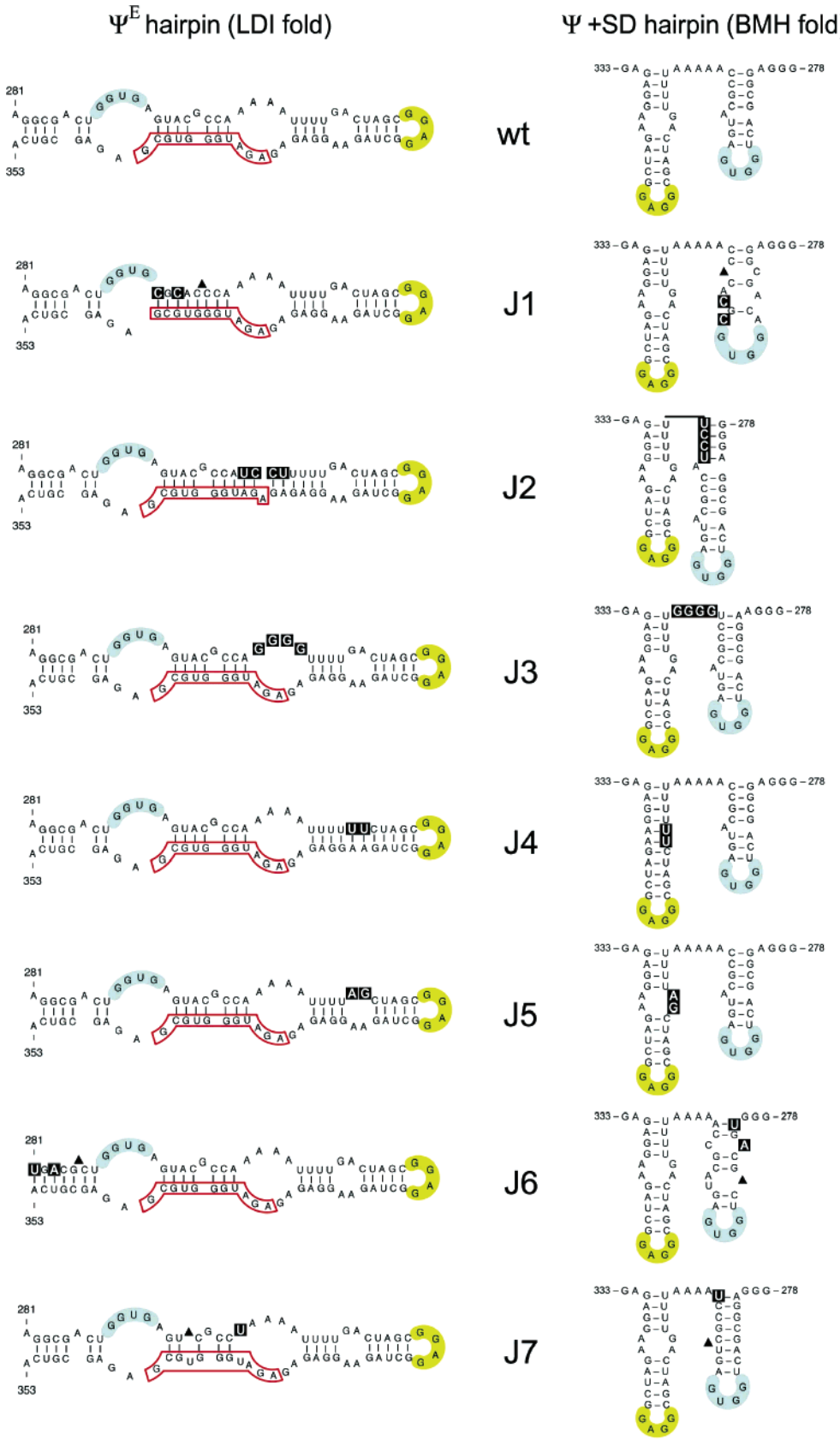

FIGURE 2: Effects of the J1−J7 mutations on the HIV-1 leader RNA structure. The Ψ^E hairpin of the LDI conformation is shown at the left, and the SD and Ψ hairpins of the BMH conformation are shown at the right. Nucleotide positions are indicated and follow the wild-type numbering. Mutated nucleotides are boxed, and deletions are denoted with a filled triangle.

Cell Culture and Transfection Assays. C33A cells, a human cervix carcinoma cell line, were grown in 24-well plates in Dulbecco's MOD Eagle's medium (DMEM) supplemented with 10% FBS, nonessential amino acids (Invitrogen), and penicillin with streptomycin. Cells were grown at 37 °C and 5% CO_2 and transfected with 200 ng of

Table 2: RNA Structure Effects of the J1−J10 Mutations

	BMH[a]			LDI[a]						
	DIS	SD	Ψ	Ψ^E	polyA−DIS	ΔG_{LDI}[b]	ΔG_{BMH}[b]	$\Delta\Delta G_{LDI-BMH}$[b]	shift to[c]	shift to[d]
wt						−119.7	−113.7	−6.0	−	−
J1		−		+		−126.7	−118.9	−7.8	LDI	LDI
J2		+		+		−128.6	−120.8	−7.8	LDI	LDI
J3						−121.1	−114.9	−6.2	LDI	ns[e]
J4			+	+		−124.6	−116.8	−7.8	LDI	LDI
J5						−122.0	−115.1	−6.9	LDI	LDI
J6		−		+		−119.8	−114.8	−5.0	BMH	LDI
J7		+		−		−120.9	−117.6	−3.3	BMH	ns[e]
J8	+				−	−118.6	−120.8	2.2	BMH	BMH
J9	+				−	−117.2	−119.4	2.2	BMH	BMH
J10					−	−116.2	−112.8	−3.4	BMH	ns[e]

[a] + and − indicate stabilization and destabilization, respectively, of RNA secondary structure. [b] ΔG values (in kilocalories per mole) as determined by Mfold. [c] Expected shift of the mutant LDI−BMH equilibrium (compared to that of the wild type) based on $\Delta\Delta G_{LDI-BMH}$ values. [d] Observed shift of the mutant LDI−BMH equilibrium (compared to that of the wild type) based on experimental RNA dimer yields (Figure 5). [e] No shift.

calcium phosphate-precipitated luciferase constructs in the presence of 5 ng of pcDNA3-Tat or pcDNA3 (*45*, *49*). pRL-CMV (5 ng) expressing *Renilla* luciferase was cotransfected as an internal control. Cells were washed with PBS 2 days after transfection and lysed in passive lysis buffer provided by the Dual-luciferase Reporter Assay System (Promega). The firefly and *Renilla* luciferase activity was determined according to the manufacturer's protocol.

RESULTS

Mutations in Ψ^E Affect the LDI−BMH Equilibrium. Previous work showed that the full-length HIV-1 leader RNA can adopt two secondary structures in vitro: LDI and BMH (*6*, *7*). The 3′-terminal 290−368 segment contributes differently to these structures. The BMH folding presents the well-known Ψ hairpin, which is significantly extended into Ψ^E in the LDI conformation (Figure 1). This Ψ^E hairpin includes the SD signal and 5′ Gag coding sequences. To determine whether alterations in the Ψ^E hairpin affected the LDI−BMH status, a set of leader mutants with a stabilized or destabilized Ψ^E hairpin, J1−J7, was designed (Figure 2 and Table 2). Leader mutants J1 and J6 were constructed to selectively stabilize Ψ^E and concomitantly destabilize SD. We therefore predicted that J1 and J6 shift the equilibrium to LDI. J7 was designed to destabilize Ψ^E and stabilize the SD hairpin and should consequently shift the equilibrium to BMH. J2 stabilizes both LDI and BMH conformations by closing an internal loop of Ψ^E and by extending SD. J3 is a control for J2: the same positions are mutated, but without an effect on the wild-type (wt) LDI and BMH structures. J4 closes the distal internal loop of Ψ and Ψ^E and thus stabilizes both the LDI and BMH conformations. In J5, the same two nucleotides are mutated as in J4, but without an RNA structure effect. The J2−J5 mutants affect the stability of both LDI and BMH structures, and consequently, the effect on the equilibrium is harder to predict. In addition, we determined if extension of the DIS hairpin would shift the LDI−BMH equilibrium. We created two mutants that extend the DIS hairpin of the BMH conformation with three consecutive base pairs: J8 and J9 (Figure 3 and Table 2). J10 combines the J8 and J9 mutations and should not extend the DIS hairpin. In addition, the J8−J10 mutants destabilize the LDI structure due to disruption of three or six base pairs in the polyA−DIS long distance interaction.

We analyzed the RNA secondary structure folding of the mutant leader RNAs with the Mfold algorithm (Table 2). The RNA structure is defined BMH if the DIS palindrome is exposed and LDI if the DIS is occluded (Figure 1). We calculated the thermodynamic stability of the LDI (ΔG_{LDI}) and BMH (ΔG_{BMH}) conformations for each mutant RNA. The difference in ΔG_{LDI} and ΔG_{BMH} ($\Delta\Delta G_{LDI-BMH}$) for the wt structures is −6.0 kcal/mol in favor of the LDI. A shift toward BMH is expected when the $\Delta\Delta G_{LDI-BMH}$ value is higher than −6.0 kcal/mol, and a shift toward LDI is expected when the value is lower. The equilibrium of the J1−J6 RNAs is shifted toward LDI, whereas that of J7 is shifted toward BMH. The proposed shift in the LDI−BMH equilibrium is most dramatic for the J8 and J9 mutations due to stabilization of the BMH structure and destabilization of the LDI structure. Mfold analysis and subsequent calculation of the $\Delta\Delta G_{LDI-BMH}$ value indicate that J8−J10 RNAs theoretically shift toward the BMH structure. The $\Delta\Delta G_{LDI-BMH}$ values of the J8 and J9 mutants even become positive, indicating that the BMH structure will be the preferred conformation (the LDI:BMH ratio is 1:1 when $\Delta\Delta G_{LDI-BMH} = 0$).

Dimerization of HIV-1 Transcripts with Mutant Ψ^E Structures. To test the effect of the J1−J10 mutations on the LDI−BMH status, radiolabeled transcripts of the wt and mutant RNA (nucleotides 1−368) were synthesized in vitro and analyzed by electrophoresis under three conditions. The migration of all transcripts was similar under denaturing conditions, although the J8 mutant shows a slightly slower migration (Figure 4A). When the same transcripts were analyzed on nondenaturing gels, the migration pattern differed significantly (panels B and C of Figure 4). Monomer LDI and BMH structures can be distinguished in a TBE-based electrophoresis (*6*, *7*). As expected, the wt monomer folds into the fast-migrating LDI structure (Figure 4B). The J1 monomer migrated even faster than the wt, suggesting that the J1 monomer folds into a more compact structure. The J2−J7 and J10 monomers migrated like the wt RNA in the TBE gel, suggesting that these mutant RNAs preferentially fold into the LDI conformation. The J8 and J9 monomers ran significantly slower than the wt RNA in the TBE gel, which is characteristic of preferential BMH folding (*7*). This result is fully consistent with the prediction of a positive $\Delta\Delta G_{LDI-BMH}$ value for these mutants.

Dimer yields reflect the shift in LDI−BMH status, since the BMH structure is dimerization-competent and the LDI structure is not (*7*). A shift toward BMH therefore translates into higher dimer yields, whereas a shift toward LDI results

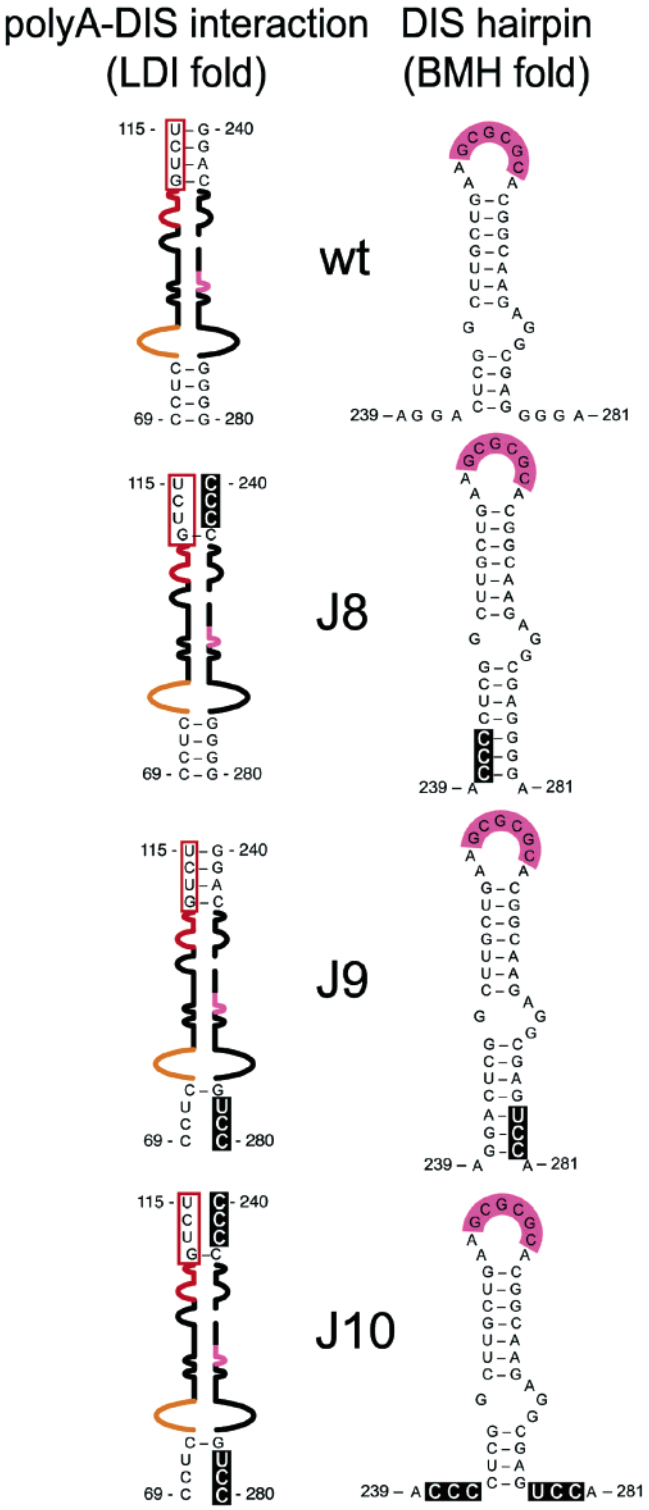

FIGURE 3: Effects of the J8−J10 mutations on the HIV-1 leader RNA structure. The polyA−DIS long distance interaction of the LDI structure is shown at the left and the DIS hairpin of the BMH structure at the right. Nucleotide positions follow the wild-type numbering. Mutated nucleotides are boxed.

in lower dimer yields. Migration of the wt and mutant RNA dimers was similar on both TBE and TBM gels, suggesting that all dimers fold into similar structures. The TBE gel shows only extended dimers (ED), whereas the TBM gel shows both kissing loop dimers and EDs (*22*, *31*, *34*, *36*, *38*). The results of several experiments were quantified to calculate the dimer yield for the wt and mutant transcripts

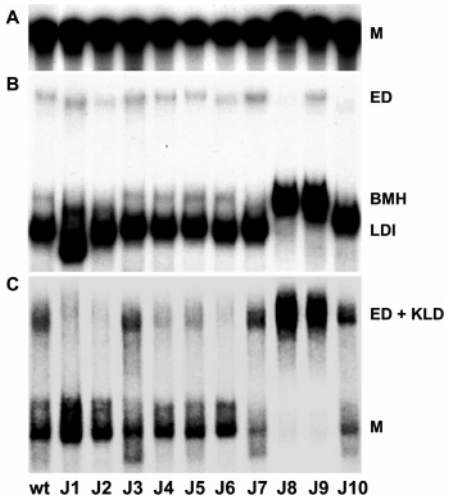

FIGURE 4: Gel electrophoresis of wild-type and J1−J10 mutant transcripts. (A) Wild-type and mutant transcripts were analyzed on a denaturing gel. (B) Migration of wt and mutant transcripts on a nondenaturing TBE gel. The migration of LDI and BMH is indicated. (C) Analysis of wt and mutant transcripts on a nondenaturing TBM gel: M, monomer; ED, extended dimer; KLD, kissing loop dimer.

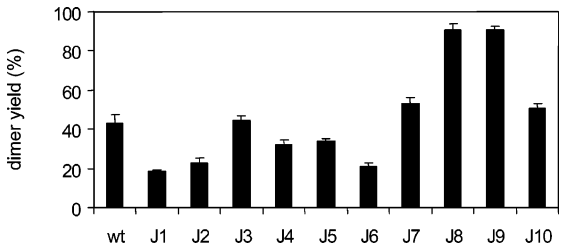

FIGURE 5: RNA dimer yield for wt and J1−J10 mutant transcripts. The graph indicates the RNA dimer yield that was quantified from four experiments as shown in Figure 4C.

(Figure 5). J1, J2, and J4−J6 transcripts dimerized less efficiently than the wt. The dimer yields of the J3, J7, and J10 transcripts did not differ significantly from that of the wt. Dimer formation of the J8 and J9 RNAs was much more efficient than wt dimer formation. These results are in overall agreement with the predicted shift in LDI−BMH equilibrium (Table 2). Therefore, the mutational design that was based on the structure models appeared to be correct. The difference in dimer yields is mainly caused by the differences in the level of kissing loop dimer formation. The yield of EDs was similar for most transcripts. We consistently measured a small but significant reduction in the level of ED formation for the J8 and J10 mutants (Figure 4B).

The LDI−BMH Status Does Not Influence Gene Expression. The *gag* initiation codon is differently folded in the LDI and BMH conformation (Figure 1). The U5−AUG duplex occludes the initiation codon in the BMH conformation. In contrast, the initiation codon is partially single-stranded in the Ψ^E hairpin of the LDI conformation. We previously suggested that formation of the U5−AUG duplex may affect the translation of the Gag protein (*6*). To test this hypothesis, we constructed wt and J1−J10 mutant luciferase reporter plasmids under control of the HIV-1 LTR promoter and leader sequences. Because Gag coding sequences contribute to the folding of Ψ^E, 75 nucleotides of the 5′-terminal sequences of the Gag coding region were included downstream of the HIV leader sequences. C33A cells were transfected with the luciferase constructs in the

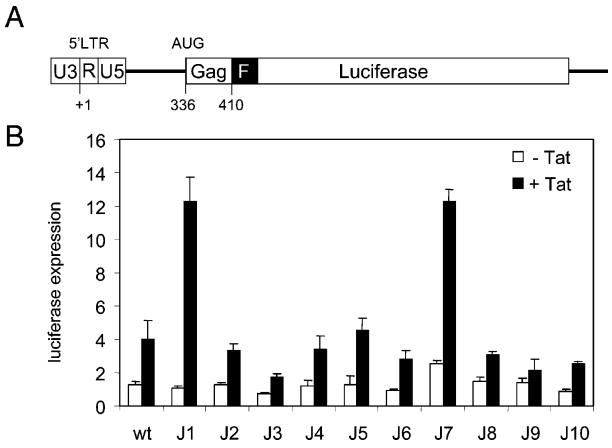

FIGURE 6: Wild-type and mutant HIV-1 leader RNA-driven luciferase expression. (A) Schematic view of the luciferase reporter. Promoter elements U3, R, and U5 are indicated. F indicates flag. AUG denotes the initiation codon; nucleotide positions of the transcription start site (+1) and the Gag coding sequences are shown. For details, see Materials and Methods. (B) Luciferase constructs were transfected into C33A cells; pcDNA3 (white bars) or pcDNA3-Tat (black bars) was cotransfected. pRL-CMV was cotransfected as an internal control. Transfections were performed in triplicate. The graph shows the level of firefly luciferase activity normalized for experimental variation, which is determined by the *Renilla* luciferase activity. Similar results were obtained in three independent experiments.

absence and presence of a Tat-expressing plasmid. The results are shown in Figure 6. In the absence of Tat, the wt and LDI−BMH mutants express similar levels of luciferase, indicating that the basal expression level is not influenced by the LDI−BMH switch. All constructs are upregulated with the transcriptional transactivator protein Tat. This is expected because all RNAs present the TAR hairpin, which is the well-characterized Tat binding site (*9*−*17*). Transcription is greatly improved as a result of the Tat−TAR interaction (*9*−*17*). In general, we did not observe an effect of the LDI or BMH mutants on luciferase expression. In the presence of Tat, the expression level of the J1 and J7 mutants was significantly increased compared to that of the wt (4- and 2.5-fold, respectively). These mutants both affected sequences in the SD region. Possibly, the increased Tat responsiveness may be due to mutations of sequences involved in leader RNA splicing (see the Discussion).

The results presented above indicate that the LDI−BMH switch does not influence the level of gene expression, including mRNA translation. To confirm this finding, we analyzed the translation efficiency of previously described U5 leader mutants s1, w1, and w2 (*6*) in which the U5−AUG duplex that occludes the start codon is affected by mutation. The U5−AUG duplex is stabilized in the s1 mutant and destabilized in the w1 and w2 mutants. The results indicated that the translation efficiency of the U5−AUG duplex mutants did not differ from that of the wt (results not shown). Thus, the strength of the U5−AUG duplex did not influence translation efficiency either.

DISCUSSION

The HIV-1 leader RNA can adopt two mutually exclusive structures: LDI and BMH. The BMH structure folds the DIS hairpin and is dimerization-competent, but this structure also base pairs the *gag* start codon in the U5−AUG long distance interaction and may thus influence the mRNA translation

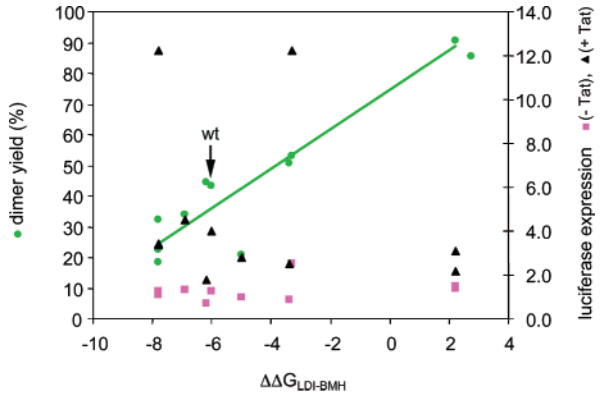

FIGURE 7: HIV-1 RNA dimer formation and not RNA translation is controlled by the LDI−BMH riboswitch. The RNA dimer yields as shown in Figure 5 are plotted against the $\Delta\Delta G_{LDI-BMH}$ values (green circles). The level of luciferase expression (without and with Tat) as shown in Figure 6 is plotted against the $\Delta\Delta G_{LDI-BMH}$ values (magenta squares and black triangles, respectively). A strong correlation was observed between the LDI−BMH equilibrium and the level of RNA dimer formation (Pearson's correlation coefficient of 0.9393).

properties. We made a set of LDI−BMH mutants and set out to test the dimerization and translation properties. We calculated the $\Delta\Delta G_{LDI-BMH}$ values based on Mfold analysis for all mutants. RNA dimer formation for the mutant transcripts was assessed in vitro. When the $\Delta\Delta G_{LDI-BMH}$ values are plotted against the RNA dimer yield, a strong correlation is apparent between these two parameters (Figure 7). We therefore conclude that the LDI−BMH status regulates RNA dimer formation.

The *gag* initiation codon is differently folded in the two leader conformations. It was therefore of interest to determine whether the J1−J10 mutant leader RNAs were affected in their capacity to initiate translation. We show that the basal level of luciferase expression from the mutant constructs did not differ significantly from that of the wt. When the $\Delta\Delta G_{LDI-BMH}$ values were plotted against the level of luciferase expression, no correlation was found between these two parameters (Figure 7). In addition, the translation efficiency of other LDI−BMH mutants that increase or decrease the base pairing strength of the U5−AUG duplex was determined. These mutants did not differ in translation efficiency either, suggesting that the LDI−BMH status does not control translation. One could argue that our assay is artificial since it does not include the viral NC protein or other HIV-1 factors that can influence the LDI−BMH switch (*7*). We therefore performed cotransfection assays with the luciferase reporter and a Gag expression plasmid. The expression levels were similar for all mutants and were not significantly influenced by the presence of Gag (results not shown). The RNA levels in our transfection system may vary due to differences in RNA stability caused by the mutations. However, preliminary Northern blot analysis and primer extension experiments suggest that this is not the case. These combined results show that the translation efficiency of the HIV-1 leader RNA is not regulated by the LDI−BMH equilibrium or by the strength of the U5−AUG duplex.

Remarkably, the expression levels of the J1 and J7 constructs differed significantly from that of the wt in the presence of Tat. The difference in luciferase expression is likely not a consequence of the altered LDI−BMH equilibrium, since the J1 and J7 mutations have an opposite effect

on the equilibrium (Figure 2 and Table 2). The J1 and J7 mutants have in common the fact that they alter sequences downstream of the 5′ major SD site. The increase in the level of luciferase expression by the J1 and J7 mutants may therefore be due to inactivation or downregulation of a splicing event at SD and a downstream splice acceptor site. In this scenario, splicing of the other constructs results in a lower level of full-length luciferase mRNA and hence a lower level of luciferase production. In the presence of Tat, J1 and J7 may block this splicing event and thus improve luciferase expression. Studies are underway to determine whether such splicing events occur in our assay system.

The RNA dimerization assays provided some new information about the formation of extended dimers (ED). J8 and J10 RNA were affected in their capacity to fold extended dimers. The DIS hairpin in the J8 RNA is extended with three consecutive base pairs. One could argue that more energy is required to melt out this stabilized DIS hairpin, resulting in a decreased level of ED formation. However, the same effect would be expected for the J9 RNA in which the DIS hairpin is similarly extended, whereas it would not be expected for the J10 control mutant that has a wt DIS hairpin. However, we observe the opposite. J10 shows a dimerization defect like J8, but J9 has a wt phenotype. The mutation that J8 and J10 have in common affects three nucleotides (240−242) upstream of the DIS hairpin (Figure 3). Possibly, these sequences are involved in the process of ED formation. Further studies are required to study the role of this novel triplet motif in ED formation.

An attractive hypothesis is that the LDI−BMH riboswitch might regulate the coordination of the competing processes of translation and packaging of the genomic HIV-1 RNA. For many years, this coordination has been the subject of scientific debate (*50*−*52*). Our data suggest that the riboswitch does not affect the level of translation directly. Mutants with either stabilized LDI or BMH structures show similar levels of protein expression. Therefore, a different mechanism likely exists that reroutes the genomic HIV-1 RNA from the translation machinery to the encapsidation machinery. One possibility is that two separate pools of genomic RNA exist in infected cells, one that is used for protein expression and one that is used for RNA packaging. However, experimental data support the existence of one multifunctional RNA population that fulfils both functions (*50*, *53*). Another option is that the translation machinery itself is inhibited during virus infection, for instance, as a consequence of cell cycle arrest (*54*, *55*). At the same time, the encapsidation machinery is built up because viral structural proteins are being produced. This will consequently shift the competition between translation and packaging toward the latter process.

Analysis of many HIV-1 leader mutants has shown that there is a strong correlation between the LDI−BMH status, RNA dimerization, and RNA packaging in vivo (*5*). The BMH fold is the dimerization-competent structure, and RNA dimers are preferentially packaged; this suggests that the BMH structure is favored over the LDI structure in RNA packaging. In addition, full-length genomic RNA is preferentially packaged over spliced RNAs. Therefore, the hypothesis that the genomic RNA stabilizes the BMH folding, possibly due to the U5−AUG interaction, is attractive (*6*). Spliced RNAs cannot fold this long distance interaction and are therefore less likely to shift their folding toward BMH. This hypothesis would also explain the recent results of Paillart and co-workers (*56*). Their in vivo RNA probing studies support the BMH fold and not the LDI fold of the HIV-1 leader. However, the authors studied only the RNA structure of the full-length leader and not that of the spliced leader variants. Thus, the putative LDI fold of spliced leader RNAs may have been missed. Furthermore, such probing studies will not easily detect minority RNA structures or structures that occur only transiently. Studies are underway to determine if the J1−J10 mutant viruses are affected in RNA packaging.

ACKNOWLEDGMENT

We thank Dr. S. Kingsman for the pSYNGP vector, Jeroen Geurtsen for technical support, and Wim van Est for artwork.

NOTE ADDED AFTER ASAP PUBLICATION

This paper was published June 2, 2005. In the sequence for the J1 r primer in Table 1, the font of the C between the two bold italic G's was changed. The corrected version was published June 6, 2005.

REFERENCES

1. Olsthoorn, R. C. L., Mertens, S., Brederode, F. T., and Bol, J. F. (1999) A conformational switch at the 3′ end of a plant virus RNA regulates viral replication, *EMBO J. 18*, 4856−4864.
2. Nudler, E., and Mironov, A. S. (2004) The riboswitch control of bacterial metabolism, *Trends Biochem. Sci. 29*, 11−17.
3. Lazinski, D. W., and Taylor, J. M. (1995) Regulation of the hepatitis delta virus ribozymes: To cleave or not to cleave? *RNA 1*, 225−233.
4. Mandal, M., and Breaker, R. R. (2004) Gene regulation by riboswitches, *Nat. Rev. Mol. Cell Biol. 5*, 451−463.
5. Ooms, M., Huthoff, H., Russell, R., Liang, C., and Berkhout, B. (2004) A riboswitch regulates RNA dimerization and packaging in human immunodeficiency virus type 1 virions, *J. Virol. 78*, 10814−10819.
6. Abbink, T. E. M., and Berkhout, B. (2003) A novel long distance base-pairing interaction in human immunodeficiency virus type 1 RNA occludes the gag start codon, *J. Biol. Chem. 278*, 11601−11611.
7. Huthoff, H., and Berkhout, B. (2001) Two alternating structures for the HIV-1 leader RNA, *RNA 7*, 143−157.
8. D'Souza, V., and Summers, M. F. (2004) Structural basis for packaging the dimeric genome of Moloney murine leukaemia virus, *Nature 431*, 586−590.
9. Puglisi, J. D., Tan, R., Calnan, B. J., Frankel, A. D., and Williamson, J. R. (1992) Conformation of the TAR RNA-arginine complex by NMR spectroscopy, *Science 257*, 76−80.
10. Aboul-ela, F., Karn, J., and Varani, G. (1995) The structure of the human immunodeficiency virus type 1 TAR RNA reveals principles of RNA recognition by Tat protein, *J. Mol. Biol. 253*, 313−332.
11. Aboul-ela, F., Karn, J., and Varani, G. (1996) Structure of HIV-1 TAR RNA in the absence of ligands reveals a novel conformation of the trinucleotide bulge, *Nucleic Acids Res. 24*, 3974−3981.
12. Ippolito, J. A., and Steitz, T. A. (1998) A 1.3-Å resolution crystal structure of the HIV-1 trans-activation response region RNA stem reveals a metal ion-dependent bulge conformation, *Proc. Natl. Acad. Sci. U.S.A. 95*, 9819−9824.
13. Berkhout, B. (1992) Structural features in TAR RNA of human and simian immunodeficiency viruses: A phylogenetic analysis, *Nucleic Acids Res. 20*, 27−31.
14. Klaver, B., and Berkhout, B. (1994) Evolution of a disrupted TAR RNA hairpin structure in the HIV-1 virus, *EMBO J. 13*, 2650−2659.
15. Dingwall, C., Ernberg, I., Gait, M. J., Green, S. M., Heaphy, S., Karn, J., Lowe, A. D., Singh, M., Skinner, M. A., and Valerio, R. (1989) Human immunodeficiency virus 1 tat protein binds trans-activating-responsive region (TAR) RNA in vitro, *Proc. Natl. Acad. Sci. U.S.A. 86*, 6925−6929.

16. Wei, P., Garber, M. E., Fang, S.-M., Fisher, W. H., and Jones, K. A. (1998) A novel CDK9-associated C-type cyclin interacts directly with HIV-1 Tat and mediates its high-affinity, loop-specific binding to TAR RNA, *Cell 92*, 451−462.
17. Berkhout, B., Silverman, R. H., and Jeang, K. T. (1989) Tat trans-activates the human immunodeficiency virus through a nascent RNA target, *Cell 59*, 273−282.
18. Klasens, B. I. F., Das, A. T., and Berkhout, B. (1998) Inhibition of polyadenylation by stable RNA secondary structure, *Nucleic Acids Res. 26*, 1870−1876.
19. Klasens, B. I. F., Thiesen, M., Virtanen, A., and Berkhout, B. (1999) The ability of the HIV-1 AAUAAA signal to bind polyadenylation factors is controlled by local RNA structure, *Nucleic Acids Res. 27*, 446−454.
20. Beerens, N., Groot, F., and Berkhout, B. (2001) Initiation of HIV-1 reverse transcription is regulated by a primer activation signal, *J. Biol. Chem. 276*, 31247−31256.
21. Beerens, N., and Berkhout, B. (2002) The tRNA primer activation signal in the HIV-1 genome is important for initiation and processive elongation of reverse transcription, *J. Virol. 76*, 2329−2339.
22. Laughrea, M., and Jette, L. (1994) A 19-nucleotide sequence upstream of the 5′ major splice donor is part of the dimerization domain of human immunodeficiency virus 1 genomic RNA, *Biochemistry 33*, 13464−13474.
23. Lever, A., Gottlinger, H., Haseltine, W., and Sodroski, J. (1989) Identification of a sequence required for efficient packaging of human immunodeficiency virus type 1 RNA into virions, *J. Virol. 63*, 4085−4087.
24. Aldovini, A., and Young, R. A. (1990) Mutations of RNA and protein sequences involved in human immunodeficiency virus type 1 packaging results in production of noninfectious virus, *J. Virol. 64*, 1920−1926.
25. Harrison, G. P., and Lever, A. M. L. (1992) The human immunodeficiency virus type 1 packaging signal and major splice donor region have a conserved stable secondary structure, *J. Virol. 66*, 4144−4153.
26. Baudin, F., Marquet, R., Isel, C., Darlix, J. L., Ehresmann, B., and Ehresmann, C. (1993) Functional sites in the 5′ region of human immunodeficiency virus type 1 RNA form defined structural domains, *J. Mol. Biol. 229*, 382−397.
27. Clavel, F., and Orenstein, J. M. (1990) A mutant of human immunodeficiency virus with reduced RNA packaging and abnormal particle morphology, *J. Virol. 64*, 5230−5234.
28. Purcell, D. F. J., and Martin, M. A. (1993) Alternative splicing of human immunodeficiency virus type 1 mRNA modulates viral protein expression, replication, and infectivity, *J. Virol. 67*, 6365−6378.
29. O'Reilly, M. M., McNally, M. T., and Beemon, K. L. (1995) Two strong 5′ splice sites and competing, suboptimal 3′ splice sites involved in alternative splicing of human immunodeficiency virus type 1 RNA, *Virology 213*, 373−385.
30. Kerwood, D. J., Cavaluzzi, M. J., and Borer, P. N. (2001) Structure of SL4 RNA from the HIV-1 packaging signal, *Biochemistry 40*, 14518−14529.
31. Skripkin, E., Paillart, J. C., Marquet, R., Ehresmann, B., and Ehresmann, C. (1994) Identification of the primary site of the human immunodeficiency virus type 1 RNA dimerization in vitro, *Proc. Natl. Acad. Sci. U.S.A. 91*, 4945−4949.
32. Paillart, J. C., Marquet, R., Skripkin, E., Ehresmann, B., and Ehresmann, C. (1994) Mutational analysis of the bipartite dimer linkage structure of human immunodeficiency virus type 1 genomic RNA, *J. Biol. Chem. 269*, 27486−27493.
33. Muriaux, D., Girard, P.-M., Bonnet-Mathoniere, B., and Paoletti, J. (1995) Dimerization of HIV-1 LAI RNA at low ionic strength, *J. Biol. Chem. 270*, 8209−8216.
34. Clever, J. L., Wong, M. L., and Parslow, T. G. (1996) Requirements for kissing-loop-mediated dimerization of human immunodeficiency virus RNA, *J. Virol. 70*, 5902−5908.
35. Haddrick, M., Lear, A. L., Cann, A. J., and Heaphy, S. (1996) Evidence that a kissing loop structure facilitates genomic RNA dimerisation in HIV-1, *J. Mol. Biol. 259*, 58−68.
36. Laughrea, M., and Jette, L. (1996) Kissing-loop model of HIV-1 genome dimerization: HIV-1 RNAs can assume alternative dimeric forms, and all sequences upstream or downstream of hairpin 248−271 are dispensable for dimer formation, *Biochemistry 35*, 1589−1598.
37. Laughrea, M., and Jette, L. (1996) HIV-1 genome dimerization: Formation kinetics and thermal stability of dimeric HIV-1LAI RNAs are not improved by the 1−232 and 296−790 regions flanking the kissing-loop domain, *Biochemistry 35*, 9366−9374.
38. Muriaux, D., Fosse, P., and Paoletti, J. (1996) A kissing complex together with a stable dimer is involved in the HIV-1 LAI RNA dimerization process in vitro, *Biochemistry 35*, 5075−5082.
39. Clever, J. L., Mirandar, D., Jr., and Parslow, T. G. (2002) RNA structure and packaging signals in the 5′ leader region of the human immunodeficiency virus type 1 genome, *J. Virol. 76*, 12381−12387.
40. Helga-Maria, C., Hammarskjold, M. L., and Rekosh, D. (1999) An intact TAR element and cytoplasmic localization are necessary for efficient packaging of human immunodeficiency virus type 1 genomic RNA, *J. Virol. 73*, 4127−4135.
41. Russell, R. S., Hu, J., Beriault, V., Mouland, A. J., Laughrea, M., Kleiman, L., Wainberg, M. A., and Liang, C. (2003) Sequences downstream of the 5′ splice donor site are required for both packaging and dimerization of human immunodeficiency virus type 1 RNA, *J. Virol. 77*, 84−96.
42. Klaver, B., and Berkhout, B. (1994) Comparison of 5′ and 3′ long terminal repeat promoter function in human immunodeficiency virus, *J. Virol. 68*, 3830−3840.
43. Berkhout, B., van Wamel, J., and Klaver, B. (1995) Requirements for DNA strand transfer during reverse transcription in mutant HIV-1 virions, *J. Mol. Biol. 252*, 59−69.
44. Beerens, N., Klaver, B., and Berkhout, B. (2000) A structured RNA motif is involved in the correct placement of the tRNALys3 primer onto the human immunodeficiency virus genome, *J. Virol. 74*, 2227−2238.
45. Verhoef, K., Koper, M., and Berkhout, B. (1997) Determination of the minimal amount of Tat activity required for human immunodeficiency virus type 1 replication, *Virology 237*, 228−236.
46. Kotsopoulou, E., Kim, V. N., Kingsman, A. J., Kingsman, S. M., and Mitrophanous, K. A. (2000) A Rev-independent human immunodeficiency virus type 1 (HIV-1)-based vector that exploits a codon-optimized HIV-1 gag-pol gene, *J. Virol. 74*, 4839−4852.
47. Mathews, D. H., Sabina, J., Zuker, M., and Turner, D. H. (1999) Expanded sequence dependence of thermodynamic parameters improves prediction of RNA secondary structure, *J. Mol. Biol. 288*, 911−940.
48. Zuker, M., and Turner, D. H. (1999) Algorithms and thermodynamics for RNA secondary structure prediction: A practical guide, in *RNA biochemistry and biotechnology* (Barciszewski, J., and Clark, B. F. C., Eds.) pp 11−43, Kluwer Academic Publishers, Dordrecht, The Netherlands.
49. Das, A. T., Klaver, B., Klasens, B. I. F., van Wamel, J. L. B., and Berkhout, B. (1997) A conserved hairpin motif in the R-U5 region of the human immunodeficiency virus type 1 RNA genome is essential for replication, *J. Virol. 71*, 2346−2356.
50. Butsch, M., and Boris-Lawrie, K. (2002) Destiny of unspliced retroviral RNA: Ribosome and/or virion? *J. Virol. 76*, 3089−3094.
51. Liang, C., Hu, J., Russell, R. S., and Wainberg, M. A. (2002) Translation of Pr55(gag) Augments Packaging of Human Immunodeficiency Virus Type 1 RNA in a Cis-Acting Manner, *AIDS Res. Hum. Retroviruses 18*, 1117−1126.
52. Poon, D. T., Chertova, E. N., and Ott, D. E. (2002) Human immunodeficiency virus type 1 preferentially encapsidates genomic RNAs that encode Pr55(Gag): Functional linkage between translation and RNA packaging, *Virology 293*, 368−378.
53. Dorman, N., and Lever, A. (2000) Comparison of viral genomic RNA sorting mechanisms in human immunodeficiency virus type 1 (HIV-1), HIV-2, and moloney murine leukemia virus, *J. Virol. 74*, 11413−11417.
54. Goh, W. C., Rogel, M. E., Kinsey, C. M., Michael, S. F., Fultz, P. N., Nowak, M. A., Hahn, B. H., and Emerman, M. (1998) HIV-1 Vpr increases viral expression by manipulation of the cell cycle: A mechanism for selection of Vpr in vivo, *Nat. Med. 4*, 65−71.
55. Gummuluru, S., and Emerman, M. (1999) Cell cycle- and Vpr-mediated regulation of human immunodeficiency virus type 1 expression in primary and transformed T-cell lines, *J. Virol. 73*, 5422−5430.
56. Paillart, J. C., Dettenhofer, M., Yu, X. F., Ehresmann, C., Ehresmann, B., and Marquet, R. (2004) First snapshots of the HIV-1 RNA structure in infected cells and in virions, *J. Biol. Chem. 279*, 48397−48403.

BI0502588